International Journal of Chemical Studies

P-ISSN 2349–8528
E-ISSN 2321–4902
IJCS 2015; 3(1): 15-22

Received: 17-04-2015
Accepted: 19-05-2015

Yadhu Krishnan
PG & Research
Dept. of Chemistry,
S.D. College, Alappuzha, India

Shine Chandran
PG & Research
Dept. of Chemistry,
S.D. College, Alappuzha, India

Nazeeha Usman
PG & Research
Dept. of Chemistry,
S.D. College, Alappuzha, India

Smitha T.R
Dept. of Chemistry,
TKMM College,
Nangiarkulangara, India

Parameswaran P.S
PG & Research
Dept. of Chemistry,
S.D. College, Alappuzha, India

Prema K.H
PG & Research
Dept. of Chemistry,
S.D. College, Alappuzha, India

Correspondence:
Prema K.H
PG & Research
Dept. of Chemistry,
S.D. College, Alappuzha, India

Processability, Mechanical and Magnetic Studies on Natural Rubber- Ferrite Composites

Yadhu Krishnan, Shine Chandran, Nazeeha Usman, Smitha T.R, Parameswaran P.S, Prema K.H

Abstract
Fine particles of gamma ferric oxide is prepared by the sol-gel method and characterized by taking XRD. Natural rubber based gamma ferric oxide composites (RFCs) with different ferrite loading are prepared by incorporating ferric oxide into the matrix according to a specific recipe. Cure characteristics and mechanical properties are determined as per ASTM standard. Magnetic studies are carried out using a vibrating sample magnetometer. This study throws light on the processability of rubber composites filled with ceramic fillers like gamma ferric oxide in natural rubber. Magnetic composites with desired magnetic properties are properly designed by tuning filler to matrix ratio.

Keywords: ferrites, gamma ferric oxide, sol-gel, natural rubber, rubber ferrite composites

1. Introduction
Ferrites and ferrite based composites are an important class of magnetic materials. Due to their immense importance, research in this area is being take place continuously. Ferrites are one of the important magnetic materials, which are stable, easily prepared and have a wide range of applications [1-3]. Ferrites in the form of ceramics and composites find applications in magnetic memories, TV yokes and in many other devices. Ceramic ferrites lack the mouldability into desired shapes which can be achieved by incorporating it in elastomers [4-8].
Composite materials provide an opportunity to design materials with required characteristics for different applications. Rubber ferrite composites (RFCs) are one such class of composites that can be prepared by incorporating ferrites in elastomer matrix. Physical properties of the matrix can be modified by the incorporation ferrites. Tailoring of magnetic and dielectric properties of ferrites to any desired level can easily be achieved through the synthesis of RFCs [9-10]. RFCs can be used as flexible magnets with excellent performance characteristics. Physico-mechanical properties of RFCs depend on various factors such as the nature of ferrite used, percolation limit, size and structure of the ferrite and interaction of the ferrites with the matrix. Both natural and synthetic rubber can be used as the matrix for RFCs. In this study NR is used as the matrix for the filling of gamma ferric oxide.
NR is being selected as the matrix for the synthesis of RFCs, for its local availability and easy processability compared to synthetic rubber. Gamma ferric oxide is selected as it has high saturation magnetization and can be prepared by a rather simple sol-gel method [11-16].

2. Materials and Methods
2.1 Preparation of gamma ferric oxide
Gamma ferric oxide particles were synthesized by dissolving hydrated ferric nitrate in ethylene glycol. The homogeneous solution is then heated at 60 ^{o}C to obtain a dry gel which is then subjected to auto combustion. The fluffy product obtained was then grained in a mortar using acetone and then dried at 100 ^{o}C in a hot air oven.

2.2 X-ray powder diffraction
Ferrite particles obtained were characterized using an X-ray powder diffraction technique (Rigaku Dmax-C) with Cu Kα radiations. The average particle size was then determined using the Debye-Sherrer formula $D= 0.9 \lambda /\beta\cos\theta$, [17] where D is the average particle size, λ is the wavelength, β is the full width at half maximum in radians and θ is the Bragg angle.

2.3 Synthesis of RFCs and Cure Characteristic Studies

Pre characterised gamma ferric oxide was then incorporated in the natural rubber matrix according to a specific recipe. The mixing was done in a two roll laboratory mill having 6 inch outside diameter with a nip gap of 1:1 inch. The speed of the slow roll is 24+0.5 rpm and the friction ratio is 1:1:2. After mixing it was moulded into thin sheets at 150 °C at their respective cure time in accordance with ASTMD 3188 using a hydraulic press.

Samples with different loading of gamma ferric oxide are designated as NRgX where X = 0,20,40,60,80 and 100 phr (parts per hundred gram of rubber) of gamma ferric oxide.

The cure characteristics of RFCs with different loading of gamma ferric oxide was determined by using ASTMD 1646, elastograph at three different temperatures viz. 140 °C, 150 °C and 160 °C.

2.4 Evaluation of Mechanical Properties

Evaluation of various mechanical properties was carried out by standard methods. The stress-strain properties of the composites were determined using Shimadzu universal testing machine model SPL 10KN at a cross head speed of 500 mm/min as per ASTM D 412-98. The tensile strength, elongation at break and modulus at 300% elongation were evaluated.

The hardness (shore A) of the composites was tested using a durometer in accordance with ASTM D2240.

2.5 Diffusion Studies

Equilibrium swelling studies of the composites were carried out in toluene. Circular samples of diameter 14.0 mm were punched from the vulcanized sheet and were allowed to swell in toluene at room temperature. At different intervals, the amount of solvent entering the sample was assessed until equilibrium was reached, as evidenced by the constant weight of the sample.

2.6 Magnetic Studies

Room temperature magnetic measurements of gamma ferric oxide and RFCs were carried out using Vibrating Sample Magnetometer (VSM) (model Lakeshore vsm 7410). Parameters like saturation magnetization (Ms), coercivity (Hc) and Retentivity (Mr) were evaluated from the hysteresis loop obtained.

3. Results and Discussion

The X-ray powder diffractogram obtained for the gamma ferric oxide is given in figure 1. The average particle size was calculated using Debye-Scherrer equation and was found to be about 19nm. The crystal planes of the ferrite are indexed in the figure.

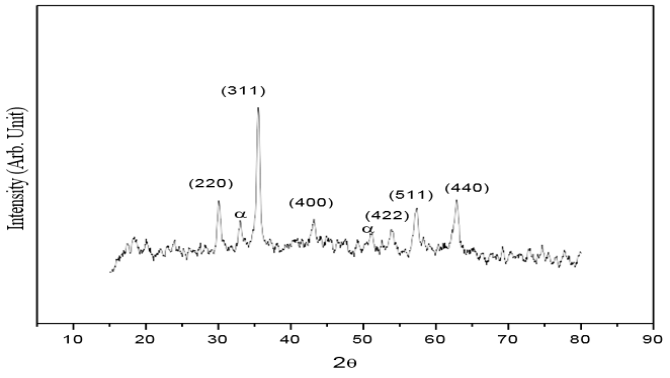

Fig 1: XRD of γ-Fe2O3

A small amount of alpha phase is also formed along with the gamma phase. This can affect the magnetic properties of γ-Fe2O3. High temperature generated during the auto combustion of gel is responsible for the formation of alpha phase.

Curing reactions were carried out at three different temperatures viz. 140 °C, 150 °C and 160 °C. Representative cure curves at these three temperatures are given in figure 2 to 4. Three regions can be seen on the vulcanizing curves for a typical accelerated sulphur vulcanization process. The first region is scorch time or induction period. That provide a safe processing time. The second region is the curing reaction period, during which the crosslinking network is formed in the rubber and hence stiffness of the rubber is increased. Third region often observed like plateau, which indicates the attainment of equilibrium of cure reaction. Sometimes even reversion or over curing may also occur during this period [18, 19].

Nature of the cure curves is similar in all the three set of cure temperatures. An induction period is well observed before the cure reaction commences. The actual curing reaction is indicated by the sudden increase in torque values. The plateau in the final stage shows the attainment of maximum curing of the elastomer.

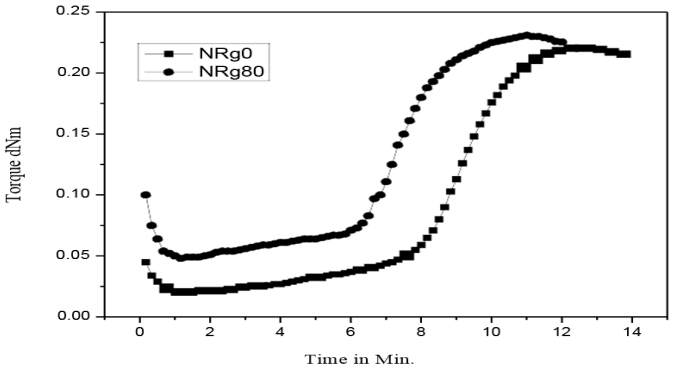

Fig 2: Representative cure curves at 140 °C

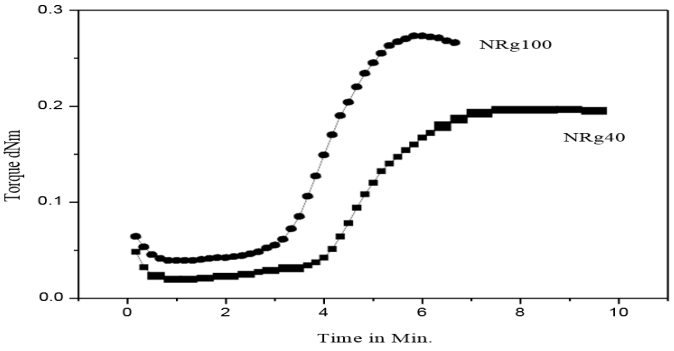

Fig 3: Cure curves for NRg40 and NRg100 at 150 °C

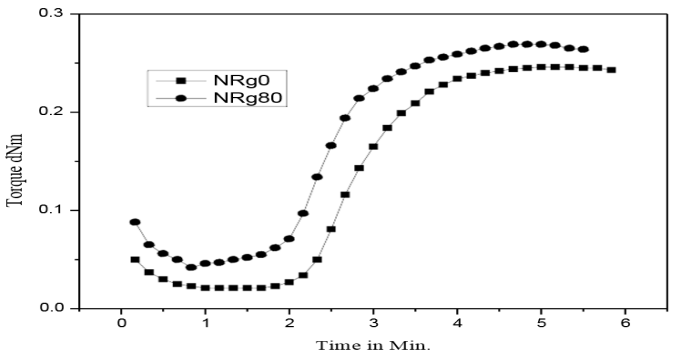

Fig 4: Representative Cure curves at 160 °C

The various curing parameters such as cure time, scorch time, maximum modulus and minimum modulus at these three temperatures are tabulated in table 1 to 3.

At 140 °C cure time of composites with different loading shows an irregular change. But at higher curing temperature cure time, gradually increases with loading upto 60 phr and decreases at higher loading. At higher filler loadings, the filler particles might have prevented the proper crosslinking between the elastomer chains.

At all these temperatures the scorch time doesn't vary much with increase in loading. So scorch time, which indicates the induction period for crosslinking reaction is not much affected by the filler loading.

Gradual increase in maximum torque is observed for all these composites at their respective cure temperature. Maximum torque is a measure of the shear modulus of the fully vulcanized rubber at the vulcanisation temperature. These values are a reflection on the filler-polymer interaction. The increase in modulus value is an indicative of increase in filler interaction with the elastomer matrix.

Minimum torque, which measures the viscosity of the unvulcanized compound is found to increase with loading in all these cases. This is according to the expectation. Inclusion of the ceramic ferrite like filler naturally increases the modulus of the elastomer.

Table 1: Cure characteristics at 140 °C

Sample	Cure time (min.)	Scorch time(min.)	Dmax.	Dmin.
NRg0	10.76	6.37	0.2208	0.0190
NRg20	9.15	5.16	0.1719	0.0220
NRg40	11.65	6.43	0.1963	0.0342
NRg60	8.87	6.32	0.2548	0.0363
NRg80	10.11	6.10	0.2325	0.0478
NRg100	12.58	6.21	0.2445	0.0625

Table 2: Cure characteristics at 150 °C

Sample	Cure time (min.)	Scorch time (min.)	Dmax.	Dmin.
NRg0	5.63	3.75	0.2208	0.0166
NRg20	5.50	3.48	0.195	0.0156
NRg40	6.45	3.81	0.197	0.0185
NRg60	9.25	3.71	0.2732	0.0281
NRg80	8.63	3.38	0.248	0.0302
NRg100	5.08	3.20	0.2725	0.0390

Table 3: Cure characteristics at 160 °C

Sample	Cure time (min.)	Scorch time (min.)	Dmax.	Dmin.
NRg0	3.73	2.28	0.2462	0.0205
NRg20	4.01	2.33	0.2318	0.0251
NRg40	4.42	2.24	0.2471	0.0295
NRg60	4.76	2.14	0.3204	0.0362
NRg80	3.45	1.94	0.2687	0.0420
NRg100	3.84	1.99	0.3353	0.0557

Change in cure time for the composites at different temperatures are studied and represented in figure 5.

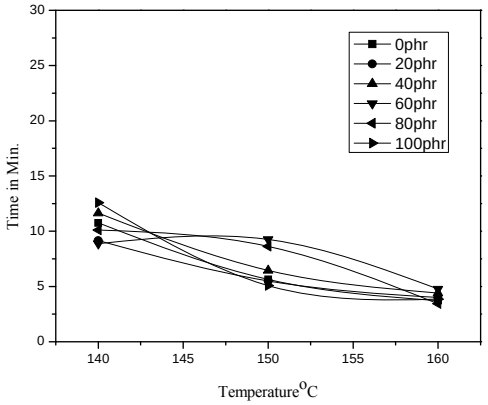

Fig 5: Variation of cure time with temperature

The cure time decreases with increase in cure temperature irrespective of the filler loading. Rate of chemical reactions is generally increases with increase in temperature. Hence, cross linking of elastomer chains, which is a chemical reaction, follows the same trend. Analogous to cure time, scorch time is also decreases with increase in cure temperature as shown in figure 6.

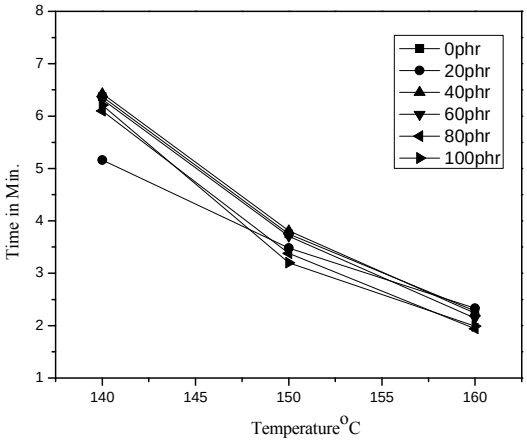

Fig 6: Variation in scorch time with cure temperature

Figures 7 and 8 show the variation in maximum and minimum torque, with respect to the change in cure temperature. Maximum torque is observed to increase with increase in temperature. Maximum torque represents the shear modulus of the vulcanisate. Hence the increase in maximum torque with temperature indicates better inclusion of the filler at higher temperature. But minimum torque, which represents the compound viscosity, is found to be minimum at 150 °C and better compounding is possible at this temperature.

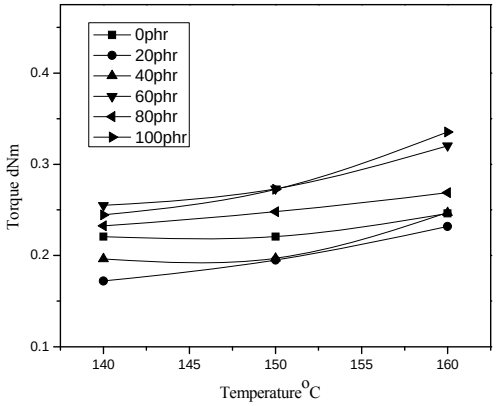

Fig 7: Variation in maximum torque with temperature for different loading of the filler

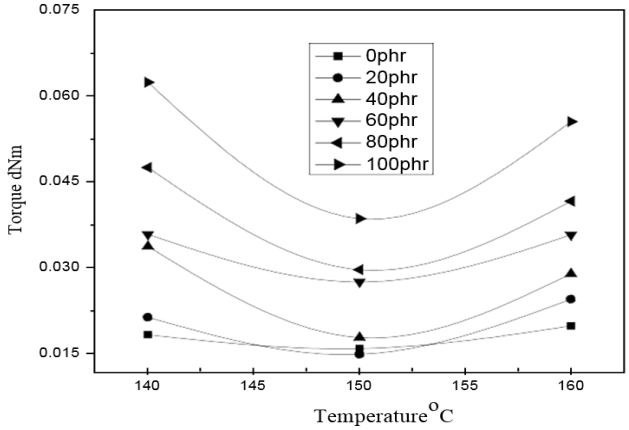

Fig 8: Variation in minimum torque with temperature for different loading of the filler

The general equation for the kinetics of a first order chemical reaction is [20-22]

$$\ln (a-x) = -kt + \ln a \quad (1)$$

For the vulcanization of rubber, cross link formation is considered as a first order chemical reaction, and the rate of reaction can be monitored by measuring the torque developed during vulcanization. The torque obtained is proportional to the modulus of the rubber. So in equation 1 the following substitutions can be made:

$$(a-x) = Mh-Mt \quad (2)$$ and

$$a = Mh-M0 \quad (3)$$

where Mh is the maximum torque, M0 is minimum torque and Mt is the torque at time t.
So the equation 1 can rewrite as

$$\ln (Mh-Mt) = -kt + \ln (Mh-M0) \quad (4)$$

Thus, if the plot of ln (Mh-Mt) against time is a straight line, it indicates the cure reaction follows first order kinetics. The cure reaction rate constant (k) is then directly obtained from the slop of the straight line plot.
The plot of ln(Mh-Mt) versus time t of the vulcanisates at different temperatures is given in figures 9, 10 and 11. The linear plots for different loadings at all these temperatures indicate that the cure reactions proceed according to first order kinetics. The slope of the straight lines gives the corresponding rate constants. Slope of the straight lines are calculated by linear fitting method and the rate constant values are tabulated in table 4.

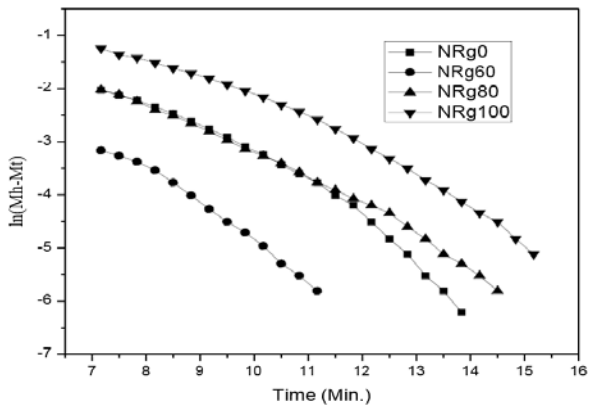

Fig 9: Plot of ln(Mh-Mt) against time at 140 °C

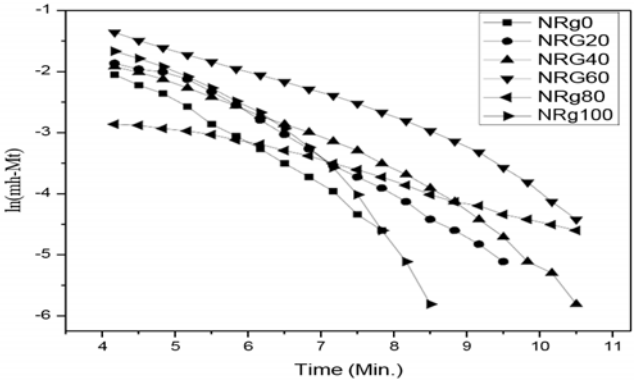

Fig 10: Plot of ln(Mh-Mt) against time at 150 °C

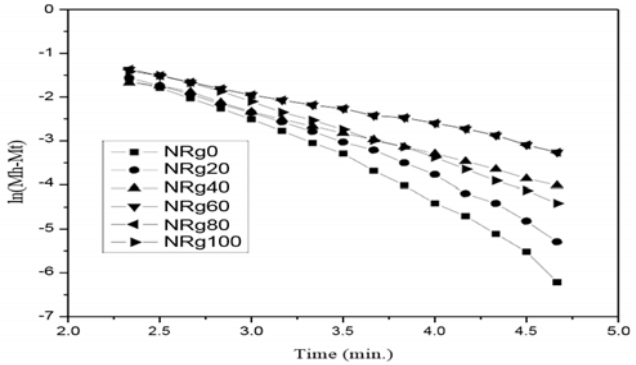

Fig 11: Plot of ln(Mh-Mt) against time at 160 °C

Table 4: Cure rate constants at different temperatures

Loading (phr)	Rate constant at 140°C	Rate constant at 150°C	Rate constant at 160°C
0	0.6486	0.7659	0.7826
20	…..	0.7644	0.733
40	……	0.6707	0.6363
60	0.8158	0.6686	0.6274
80	0.8372	0.6618	0.6182
100	0.8636	0.625	0.540

Cure rate constant is found to increase with increase in filler content at 140 °C. But at higher temperatures it is found to decrease with increase in loading. Cure rate constant for neat rubber is found to increase with increase in cure temperature. But for composites with different filler content the rate constant is found to decrease with increase in temperature. This indicates that gamma ferric oxide particle may affect the rate of cure reaction. However the mechanism of cure reaction is not affected by these fillers.
Figure 12 represents the changes in the tensile strength of rubber vulcanisates with filler loading. Tensile strength of the composites are found to increase with loading upto 40phr. Above this it is found to decrease, however the values are still comparable with that of gum vulcanisate. The increase in tensile strength of the composites speaks of the reinforcing nature of the filler. The enhancement in tensile strength is due to the larger surface area of the fillers since the fillers are in the ultrafine regime (size~ 20 nm). As the particle size decreases the interface area between the filler and the elastomer increases, which leads to better reinforcement characteristics.
Figure 13 shows the variation of elongation at break with filler loading. Here also the value is found to be maximumm for 40phr loading. Increase in elongation value with loading is due to the increase in the stress bearing capacity of the filler-matrix interface. This once again supports the reinforcing nature of ferrite fillers.

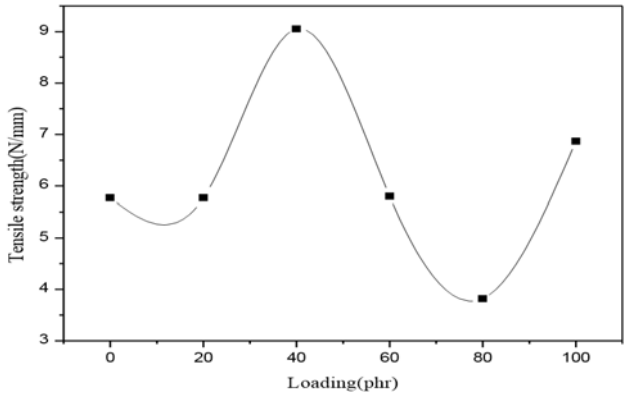

Fig 12: Variation of tensile strength with loading

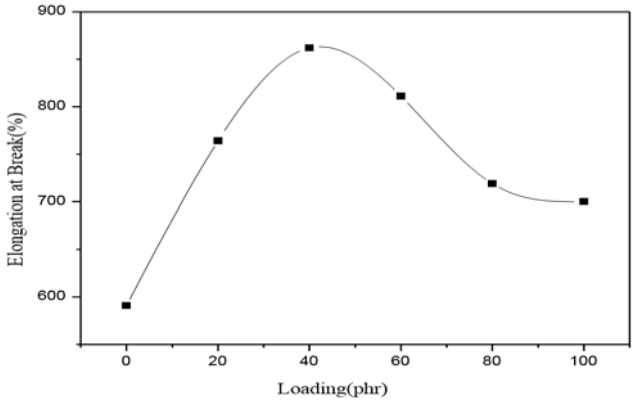

Fig 13: Variation of elongation at break with filler loading

Figure 14 shows the variation of modulus at 100%, 200%, 300% elongation. Between the loadings 20 to 80phr maximum value is observed for 40phr. All these studies thus indicate that the percolation limit of γ-Fe2O3 filler in natural rubber is about 40-60phr. However, higher loading composites still retain comparable results with that of gum vulcanisates. Thus vulcanisates with higher loading is recommended for their higher magnetic properties which are discussed in the forthcoming sections.

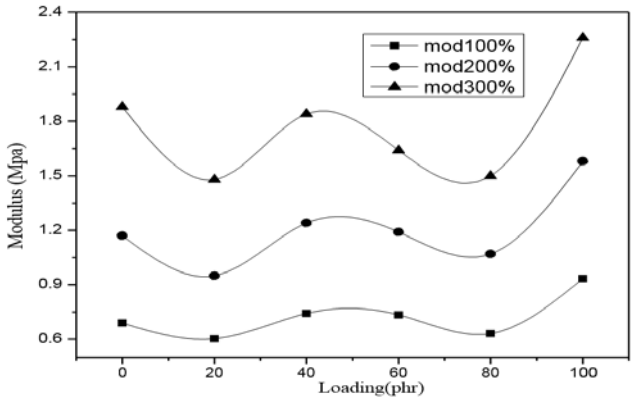

Fig 14: Variation of modulus at 100%, 200%, 300% elongation

Figure 15 exhibit the hardness values of the composites. Hardness represents a measure of modulus at low strains. Hence Hardness values with no doubt increases with increase in filler loading.

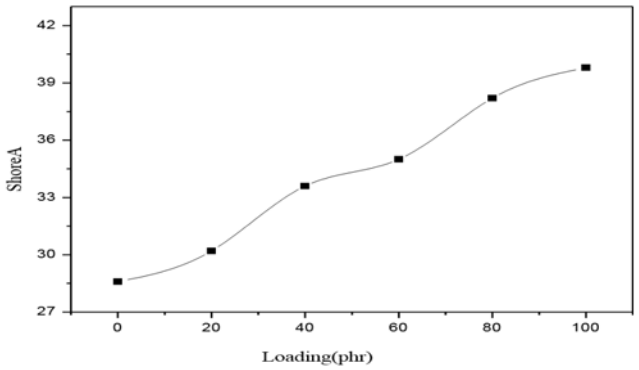

Fig 15: Variation of hardness with filler loading

Sorption characteristics of the composites were carried out as per the reported methods and various sorption characteristics such as diffusion, sorption and permeation coefficients are calculated according to the equations 5 to 7.

$$D = \pi\left(\frac{h\theta}{4Q_{\infty}}\right)^2 \quad 5$$

$$S = \frac{M_{\infty}}{M_0} \quad 6$$

$$P = DS \quad 7$$

The sorption curves of the gum vulcanisates and ferrite filled vulcanisates at room temperature are presented in figure 16. It can be seen from the sorption curves of the samples that the initial swelling rate is very high owing to the large concentration gradient. This keeps the polymer sample under intense solvent stress. As the concentration gradient decreases with advancing swelling, the swelling rate decreases and the concentration difference becomes negligible at equilibrium swelling. The equilibrium mole% uptake is given in table 5. It is found to decrease with increase in filler amount. The decrease in mole% uptake is due to the decrease in volume fraction of elastomer with loading.

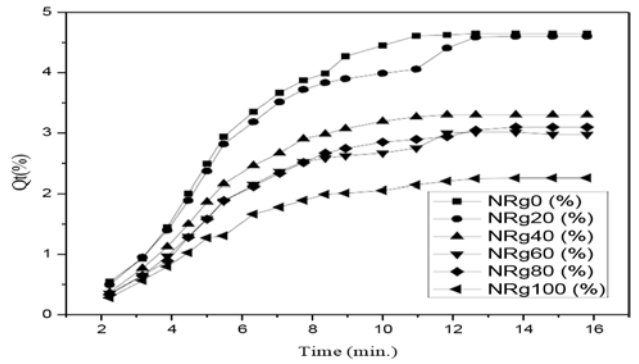

Fig 16: Sorption curves for the composites

Table 5: Equilibrium mole percentage uptake

Loading (phr)	Q∞ (%)	n
0	4.653	0.9620
20	4.606	0.9733
40	3.306	0.9397
60	2.981	0.9424
80	3.102	0.9744
100	2.257	0.8825

The mechanism of penetrant transport into the elastomer network can be analyzed using an empirical relation of the form

$$\log Qt/Q\infty = \log k + n \log t \quad (8)$$

where Qt is the mole % uptake at time t, Q∞ is the equilibrium mole % uptake and k is a constant. Value of n determines the mode of transport of solvent through rubber compound which depends upon many factors such as chemical nature of rubber and vulcanizing agents dimension and shape of the filler, rubber-filler compatibility and interfacial adhesion. The liquid diffusion can be Fickian, non-Fickian or anomalous, depending upon the value of 'n'. When n is 0.5, the mechanism is known as Fickian. Here the rate of polymer chain relaxation is higher compared to the diffusion rate of penetrant. When n = 1, the transport process corresponds to a mechanism where chain relaxation is slower than liquid diffusion, which is expected for rigid polymers. When the value of n is in between 0.5 and 1 the transport behaviour is termed as anomalous where rearrangement of polymer molecules occurs at a comparable rate to that of the change of concentration.

Value of 'n' is tabulated in table 5. Here the value of 'n' in all cases is greater than 0.5 and almost near to 1. This indicates that the penetration mechanism of toluene through the matrix in RFCs is non fickain.

During diffusion process the polymer swells and mass flow may takes place in addition to the molecular diffusion. Diffusion coefficients which have been corrected for mass flow are termed as intrinsic diffusion.

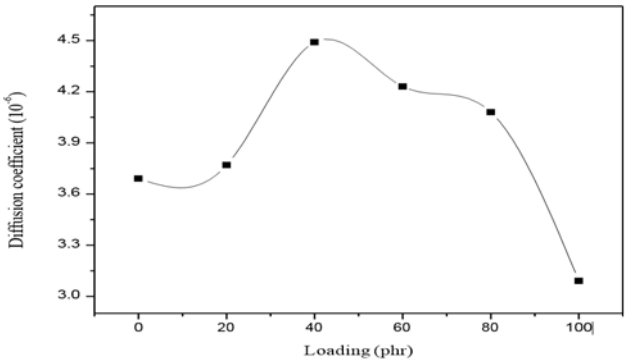

Fig 17: Diffusion coefficients of γ-Fe2O3 filled composites

Figure 17 shows the variation of the intrinsic diffusion coefficient of the composites. As the loading increases the diffusion coefficient increases upto 40phr and then decreases. Transport of penetrant molecules, through polymer proceeds via a two stage sorption, diffusion process. At first the penetrant molecules are sorbed by the polymer followed by diffusion. Diffusivity is a kinetic parameter which depends on the polymer segmental mobility. The increase in diffusion coefficient at lower loading of filler indicates that the sorption of the penetrant by the polymer chain is not affected by the presence of filler. At higher concentration filler particles restrict the diffusion of the solvent molecule through the elastomer. This decreases the diffusion coefficient at higher loading.

The variation of sorption coefficient is plotted in figure 18, which decreases with loading. As the loading increases the volume fraction of polymer decreases, consequently sorption decreases as the available polymer surface for diffusion decreases.

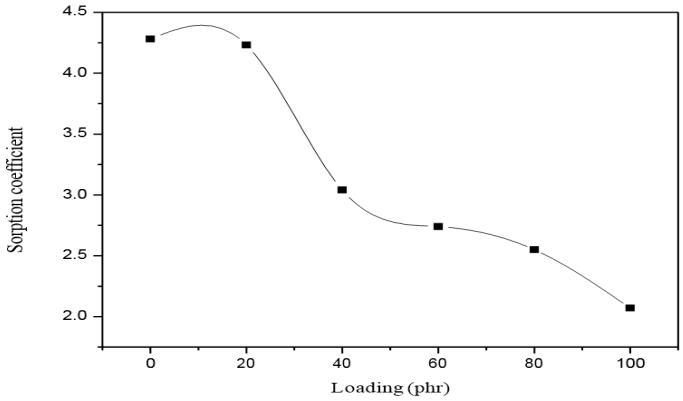

Fig 18: Variation of sorption coefficient with loading

Figure 19 shows the variation of the permeation coefficient of the composites with loading. Permeation coefficient decreases with loading as in the case of sorption coefficient. Permeation coefficient is a characteristic parameter reflecting collective processes of diffusion and sorption. Hence it can be concluded that in this particular set of composites the permeability is controlled significantly by the process of sorption.

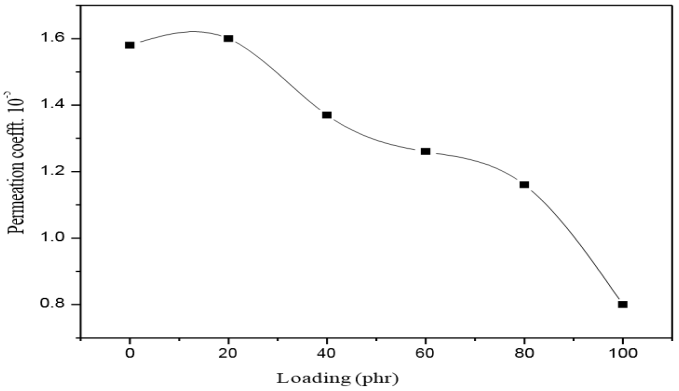

Fig 19: Variation of permeation coefficient

Figure 20 represents the hysteresis loop of the RFCs and that of gamma ferric oxide. Various magnetic parameters such as saturation magnetization, magnetic remanence and coercivity are then determined and tabulated in table 6.

Coercivity is the field required to bring the saturation magnetization to zero. From the table it is clear that the coercivity of the composites is not much differed from the value of ferric oxide. However slight increase is observed for composite with 40 phr loading.

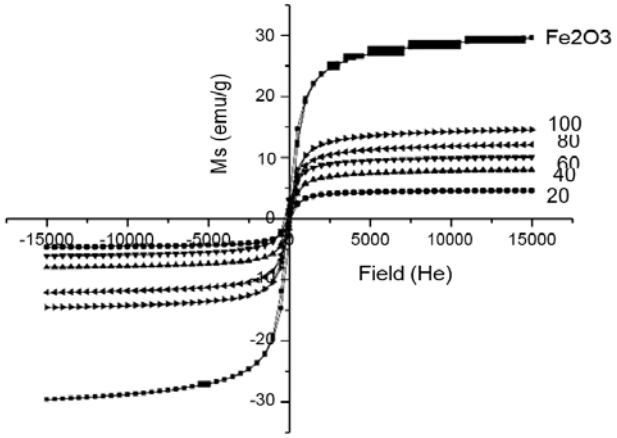

Fig 20: Hysteresis loops of γ-Fe2O3 and composites with different loading of γ-Fe2O3

Table 6: Magnetic characteristics of γ-Fe2O3 and composites

Sample	He(Oe)	Mr(emu/g)	Calculated Mr	Ms(emu/g)
Fe2O3	100.1	3.01	…..	29.6
NRg20	101.0	0.58	0.46	4.64
NRg40	106.8	1.10	0.79	7.99
NRg60	102.4	1.02	1.05	10.06
NRg80	102.0	1.52	1.26	12.11
NRg100	105.0	1.89	1.424	14.48

Regular increase in saturation magnetization is observed for the composites with loading. Since saturation magnetization of these magnetic composites is a filler dependent phenomenon the Ms value of composites can be tailored with the proper selection of the ferrite and amount of the magnetic filler within the matrix. If the Ms value of the filler is known a simple mixture equation of the general form (equation 9) involving the weight fractions of the filler can be employed to calculate the Ms of the composites [23].

$$MC = W1M1+W2M2 \quad (9)$$

Where MC is the saturation magnetization of the composite, W1 is the weight fraction of the filler, M1 is the saturation magnetization of the filler, W2 is the weight fraction of the polymer matrix and M2 is the saturation magnetization of the matrix. Since the matrix used for the preparation of the composite is non magnetic equation 9 can be reduced to the following form

$$MRFC = W1M1 \quad (10)$$

Figure 21 gives a comparison of calculated Ms value with that of experimental value.

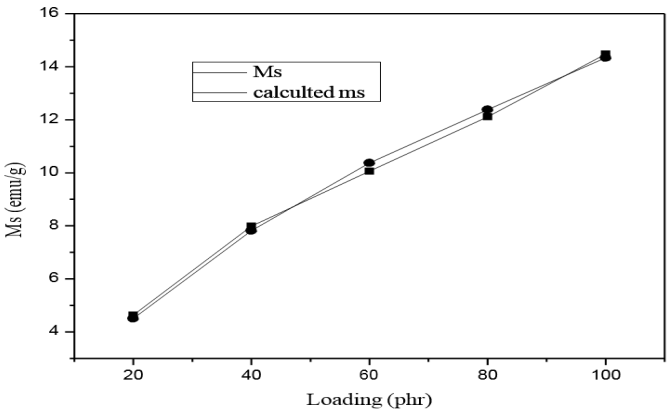

Fig 21: Experimental and calculated values of saturation magnetization

Remanent magnetization as given in table 5, exhibit a regular increase with loading. As it is a filler dependant phenomena the result obtained is in good agreement with the expectation. Remanant magnetization values are calculated using a similar equation as that of equation 10. Calculated values are found to be less than that of the experimental value. This may be due to the presence elastomer matrix which may prevent the reversion of magnetization.

4. Conclusion

γ-Fe2O3 in the nano region is synthesized by sol-gel method. The size of the ferrite particle is ~ 19 nm. NR based composites in the different filler loadings were synthesized and their properties were studied. Cure characteristics of the composites shows that better compounding is possible at 150 °C. Cure kinetic studies indicate a first order kinetics for cure reactions. However, the incorporation of γ-Fe2O3 affects the rate of cure reaction. The improvement in the mechanical properties confirm the reinforcing nature of γ-Fe2O3 in NR matix. Mechanical properties are maximum at 40 phr loading. Sorption studies indicate non-fickain mechanism for the penetration of solvent through the composites. Inclusion of ceramic filler restrict the free movement of solvent through the matrix. A gradual increase in Ms value is observed with filler loading. Thus, elastic, magnetic composites with desired magnetic property can be achieved by the incorporation of γ-Fe2O3 in NR.

5. Acknowledgments

This work is supported by the grant sanctioned by the Kerala State Council for Science, technology and Environment (KSCSTE), Thiruvananthapuram under the plan of Students Project (SPS). We acknowledge SAIF, IIT Madras and SAIF, CUSAT for the VSM and XRD results respectively. Our sincere thanks to Common Facility Service Centre, Changanacherry, for the preparation of composite materials at this centre.

6. References

1. Cullity BD. 'Magnetic Materials', Addison Wesley, London, 1972, 181-202.
2. Snelling EC, Giles AD. 'Ferrites for Inductors and transformers', Reseach Studies Press, UK, 1983, 29-72.
3. Smit J, Win HPG. 'Ferrites', Philips Technical library, The Netherlands, 1959, 136:175.
4. Malini KA, Kurian P, Anantharaman MR. Loading dependence similarities on the cure time and mechanical properties of rubber ferrite composites containing nickel zinc ferrite, Materials Letters, 2003; 57:3381-3386.
5. Soloman MA, Philip K, Anatharaman MR, Joy PA. Magnetic and processability studies of nitrile rubber vulcanisates containing barium ferrite and carbon black, Indian journal of Chemical technology 2005; 12:582-587.
6. Prema KH, Philip Kurian, Joy PA, Anatharaman MR. Physic mechanical and magnetic properties of neoprene based rubber ferrite composites, Polymer- Plastic Technology and Engineering 2008; 47:137-146.
7. Soloman MA, Philip K, Anatharaman MR, Joy PA. Evaluation of the magnetic and mechanical properties of rubber ferrite composites containing strontium ferrite, Polymer-Plastic Technology and Engineering 2004; 43:1013-1028.
8. Annadurai P, Mallick AK, Tripathy DK. Studies on microwave shielding materials based on ferrite- and carbon black-filled EPDM rubber in the X-band frequency. Journal of Applied Polymer Science 2002; 83(1):145-150.
9. Anatharaman MR, Malini KA, Sindhu S, Mohammed EM, Date SK, Kulkarni SD *et al.* Tailoring magnetic and dielectric properties of rubber ferrite composites containing mixed ferrites. Bull Mater Sci 2001; 24(6):623-631.
10. Soloman MA, Philip K, Anatharaman MR, Joy PA. Processability and magnetic properties of rubber ferrite composites containing barium ferrite. International Journal of Polymeric Materials 2004; 53:565-575.
11. Hasany SF, Ahmed I, Rajan J, Rehman A. Systematic Review of the Preparation Techniques of Iron Oxide Magnetic Nanoparticles, Nanoscience and Nanotechnology 2012; 2(6):148-158.

12. Mohapatra M. Anand S. Synthesis and applications of nano-structured iron oxides/hydroxides, International Journal of Engineering, Science and Technology 2010; 2(8):127-146.
13. Rane KS, Verenkar VMS. Synthesis of ferrite grade γ-Fe2O3, Bull. Mater. Sci 2001; 24(1):39-45.
14. Song J, MA Zhen-Ye, Cheng LI, WU Ru-Jun. Synthesis of ferric oxide nano particles with controllable crystal phases by salt assisted combustion method. Journal of Inorganic Materials 2010; 25(7):780-784.
15. Zhenxing Y, Zhou JI, Longtu LI, Hongguo Z, Zhilum G. Synthesis of nanocrystalline NiCuZn ferrite powders by sol-gel auto-combustion method. Journal of Magnetism and Magnetic Materials 2000; 208(1-2):55-60.
16. Souilah Zahi, Mansor Hashim, Daud AR. Preparation of Ni-Zn-Cu ferrite particles by sol-gel technique. Materials letters 2006; 60(23):2803-2806.
17. Dilip K, Sharon M. 'Characterisation of Nano-Materials by X- Ray Diffraction' MONAD Nanotech Pvt. Ltd. Mumbai, 2007, 84-95.
18. Sui G, Zhong WH, Yang XP, Yu YH. Curing kinetics and mechanical behavior of natural rubber reinforced with pretreated carbon nanotubes, Materials Science and Engineering A 2008; 485:524-531.
19. Dongcheol C, Abdul KM, Baik-Hwan Cho, Yang-Il Huh, Changwoon Nah. Vulcanization Kinetics of Nitrile Rubber/Layered Clay Nanocomposites. Journal of Applied polymer Science 2005; 98:1688-1696.
20. Mathew G, Nah C, Rhee JM, Singh RP. Multifiller-matrix Adhesion Effects in Epoxidized Natural Rubber. Journal of Elastomers and Plastics 2006; 38:43-62.
21. Abi SA, Thomas S, Joseph K, Marianti N, Barkoula, Karger KJ. Sulphur vulcanization of styrene butadiene rubber using new binary accelerator systems. Journal of Elastomers and Plastics 2003; 35(1):29-53.
22. Mathew G, Rhee JM, Lee YS, Park DH, Nah C, Cure kinetics of ethylene acrylate rubber/clay nanocomposites. Journal of Industrial and Engineering Chemistry 2008: 14:60-65.
23. Malini KA, Mohammed EM, Sindhu S, Joy PA, Date SK, Kulkarni SD *et al.* Magnetic and processability studies on rubber ferrite composites based on natural rubber and mixed ferrites. J Mater Sci 2001; 36(23):5551-5557.